Refinement of Eutectic Si in High Purity Al-5Si Alloys with Combined Ca and P Additions

THOMAS HARTMUT LUDWIG, JIEHUA LI, PAUL LOUIS SCHAFFER, PETER SCHUMACHER, and LARS ARNBERG

The effects of combined additions of Ca and P on the eutectic Si in a series of high purity Al-5 wt pct Si alloys have been investigated with the entrained droplet technique and complementary sets of conventional castings. Differential scanning calorimetry (DSC) and thermal analysis were used to investigate the eutectic droplet undercooling and the recalescence undercooling, respectively. Optical microscopy, SEM, EPMA, and TEM were employed to characterize the resultant microstructures. It was found that 250 ppm Ca addition to Al-5Si wt pct alloys with higher P contents leads to a significant increase of the eutectic droplet undercooling. For low or moderate cooling rates, the TEM results underline that Ca additions do not promote Si twinning. Thus, a higher twin density cannot be expected in Ca containing Al-Si alloys after, *e.g.*, sand casting. Consequently, a refinement of the eutectic Si from coarse flake-like to fine plate-like structure, rather than a modification of the eutectic Si to a fibrous morphology, was achieved. This strongly indicates that the main purpose of Ca additions is to counteract the coarsening effect of the eutectic Si imposed by higher P concentrations. Significant multiple Si twinning was observed in melt-spun condition; however, this can be attributed to the higher cooling rate. After DSC heating (slow cooling), most of Si twins disappeared. Thus, the well-accepted impurity-induced twinning mechanism may be not valid in the case of Ca addition. The possible refinement mechanisms were discussed in terms of nucleation and growth of eutectic Si. We propose that the pre-eutectic Al_2Si_2Ca phase and preferential formation of Ca_3P_2 deactivate impurity particles, most likely AlP, poisoning the nucleation sites for eutectic Si.

DOI: 10.1007/s11661-014-2585-6

I. INTRODUCTION

MODIFICATION of hypoeutectic Al-Si alloys has been extensively used in the Al foundry industry in order to induce a structural transformation of the eutectic Si from a coarse flake-like to a fine fibrous morphology. This is beneficial as it improves the mechanical properties of the final cast part. Modification can generally be achieved by applying a rapid cooling rate (quench modification) or by adding certain trace elements (chemical modification). Sr, Na, Ba, Eu, and Ca are the elements that are presumed to modify the coarse plate-shaped eutectic Si to a fibrous structure.[1] It is generally established that modification occurs according to the impurity induced twinning (IIT)[2] and the twin-plane re-entrant edge growth mechanism (TPRE).[3] These mechanisms involve preferential adsorption of impurity atoms at self-perpetuating re-entrant corners and thus poisoning of potent sites for attachment of Si atoms leading to more frequent branching of the growing Si crystal and consequently yielding significant Si twinning.

According to IIT, the atomic radius ratio of the element Ca($r_{Ca}/r_{Si} = 1.68$)[4] is very close to the ideal atomic radius ratio (1.646).[2] Hence it is expected that Ca can be adsorbed at the growing solid–liquid interfaces to promote Si twinning, and thus results in a fibrous Si morphology. However, previous research on the modification potential of Ca in hypo- or near-eutectic Al-Si alloys appears to be, to some extent, inconclusive. It is reported that a well-modified Al-Si eutectic can be achieved with Ca additions,[5–10] and its modification effect remained even after remelting.[10,11] In contrast, Abdollahi[12] emphasizes that a fully fibrous eutectic Si cannot be obtained with Ca at low cooling rates (*i.e.*, sand casting). It was concluded that in order to completely transform Si platelets into Si fibers, it needs the assistance of high cooling rates (*i.e.*, die casting) in addition to added Ca. This poses the question; how can one distinguish with a high degree of certainty whether or not the modification is caused by high cooling rates (quenching modification) or chemical modification? Previous investigations on the modification potential of Sb, Y, and Yb summarize[5,13–15] that

THOMAS HARTMUT LUDWIG, Project Engineer, is with the Hydro Aluminium, Årdal Metal Plant, 6882 Øvre Årdal, Norway. Contact e-mail: thomas.ludwig@hydro.com JIEHUA LI, Senior Lecturer, Chair of Casting Research, is with the Department of Metallurgy, University of Leoben, 8700 Leoben, Austria. PAUL LOUIS SCHAFFER, Research Scientist, is with the Bureau Veritas, Brisbane, Australia, and also with the Hydro Aluminium, Research and Technology Development, 6601 Sunndalsora, Norway. PETER SCHUMACHER, Professor, Chair of Casting Research, is with the Department of Metallurgy, University of Leoben, and also with the Austrian Foundry Research Institute, Park Str. 18, 8700 Leoben, Austria. LARS ARNBERG, Professor, is with the Department of Materials Science and Engineering, Norwegian University of Science and Technology, 7491 Trondheim, Norway.

Manuscript submitted April 8, 2014.

Published online: 16 October 2014

these elements solely refine the eutectic Si, even though their atomic radii ratio is also close to the ideal atomic radii ratio.[4] All these results demonstrate that the ratio of atomic radii alone is not sufficient to predict the modification effect. Other factors, *i.e.*, the partition or diffusion behavior of the impurity element into Si may also be considered.

The adsorption of Ca atoms on growing Si surfaces resulting in more significant Si twinning is also discussed in the literature. This debate originates from a segregation study with NanoSIMS,[16] where Ca was detected to segregate preferably to the Al matrix, rather than to the eutectic Si, strongly indicating that IIT may be not valid in the case of Ca additions to Al-Si alloys. It therefore appears that other working mechanisms occur, *e.g.*, interaction of Ca with other impurity elements takes place. Impurity elements, *e.g.*, P, are reported to have a noticeable influence on the solidification mode and the modification effects of the Al-Si eutectic. It is claimed that the main purpose of the Ca addition is to reduce impurities (*i.e.*, AlP) acting as nucleation sites for eutectic Si.[17,18] The addition of P to Al melts leads to the formation of the thermally stable AlP compound present as spheroids or as platelets at temperatures well above the liquidus temperature of Al alloys prior to the first solid in the melt[19,20] owed to the low solid solubility of P in Al (0.02 ppm P at 933 K (660 °C)[21]).

The formation of AlP is beneficial in hypereutectic Al-Si alloys because it decreases the size of primary Si and leads to a homogenous distribution of primary Si. In hypoeutectic Al-Si alloys, however, higher fractions of AlP compounds are regarded detrimental for the alloys performance because the eutectic Si undergoes a significant coarsening. Nogita *et al.*[22] identified the AlP particles as the key impurities acting as nucleation sites for Si based on their crystallographic orientation relationship. It is proposed that Si nucleates epitaxially with a cube-to-cube relationship on the pre-existing AlP particles or on AlP patches which form from dissolved P in the residual liquid along the solute boundary layer ahead of the growing primary Al dendrites. In this case, the Si crystals resemble the polyhedral morphology of primary Si crystals from where the solidification of eutectic commences yielding a coarse Al-Si eutectic structure. Therefore, reducing the amount of AlP particles appears to be inevitable in commercial purity Al-Si alloys to reduce the size of Si platelets.[6,23–25] This can either be achieved by formation of intermetallics which themselves might nucleate on AlP or by formation of P bearing compounds on expense of dissolved P in the melt. Alternatively, the usage of high purity (HP) Al and Si materials or the application of a superheat treatment of the Al-Si alloys [*i.e.*, higher than 1273 K (1000 °C)] also reduces the potency of AlP. Following the remarks of Lescuyer *et al.*,[19] a well-modified eutectic Si structure can be expected when the superheated alloy is quickly cooled from superheat-to pouring temperature. The modification of the eutectic Si in superheated Al-Si alloys might then be due to two mechanisms: the dissolution of (i) AlP particles and (ii) Si clusters or crystalline Si particles[26,27] which may not re-precipitate excessively upon rapid cooling.

Despite the comprehensive research on the modification of eutectic Si, to date, there is still a lack of a systematic investigation on the effects of Ca addition to Al-Si alloys with the presence of different trace amounts of P. In this paper, a series of HP Al-5 wt pct Si alloys with combined Ca and P additions have been investigated using the entrained droplet technique developed by Wang and Smith.[28] Entrainment of eutectic droplets has proven to be a reliable method to investigate the nucleation kinetics of the Al-Si eutectic in the presence of trace impurity elements.[29] In order to further elucidate the effect of combined Ca and P additions on the Al-Si eutectic, standard thermal analysis was employed for conventional cast samples to investigate the eutectic undercooling. The trends of the characteristic undercooling temperatures obtained with these two different casting techniques are discussed and related to microstructure evaluations with optical microscopy, SEM, EPMA, and TEM.

II. EXPERIMENTAL METHOD

A series of Al-5Si alloys (wt pct is used throughout the paper unless stated otherwise) were prepared using HP aluminum (5N grade, 99.998) and HP silicon chips (6N grade). P and Ca additions in the nominal range of 0.5 to 10 ppm and 25 to 250 ppm were made using Al-16 Cu-1.4 P master alloy rods and Al-5 Ca master alloy produced from Al5N grade Al and metallic Ca, respectively. The nominal alloy compositions used in the present investigation are given in Table I.

Ingots of about 3 kg were produced for each alloy composition by electric resistance melting of the charge material in a boron-nitride-coated clay-graphite crucible at 1023 K (750 °C). The chemical composition of the investigated alloys was determined with a Finnigan ELEMENT GD glow-discharge mass-spectrometer (GD-MS). This spectroscopy technique allows quantitative trace element analysis in the low-ppb range. As summarized in Table I, the following isotopes were measured ^{27}Al, ^{28}Si, ^{31}P, and ^{44}Ca.

About 1 kg of ingot material was remelted in an electric resistance furnace at 1023 K (750 °C) to conduct thermal analysis measurements according to the

Table I. Chemical Composition of Al-5Si Alloys with Combined Ca and P Addition as Measured by GD-MS in ppm

	Nominal Composition (ppm)		Measured Composition (ppm)			
Alloy	Ca	P	Ca	P	Si × 10^4	Al
Reference	>0.1	0.5	>0.1	0.5	5	bal.
	25	0.5	21.4	0.5	5	bal.
		3.0	23.2	3.0	5	
		10	22.6	7.8	5	
	250	0.5	245	0.5	5	bal.
		3.0	220	3.5	5	
		10	249	8.8	5	

Quik-Cup® method. This set-up yields a cooling rate prior to solidification of 10 K/min. The recalescence undercooling of the eutectic reaction ΔT_{eu} was defined as the temperature difference between the growth temperature of the eutectic, $T_{G,eu}$ and the minimum temperature of the eutectic, $T_{min,eu}$. An optical microscope was used to analyze the microstructure of conventional cast samples at a location approximately halfway up the Quik-cup in the vicinity of the thermal couple tip.

For melt spinning, ingots of about 12 g were placed in a quartz glass with an orifice of ∅1 mm. They were then remelted under high vacuum conditions and ejected onto to a rotating copper wheel with a rotational speed of 20 m/s. The thermal history of the ribbons was monitored using a power compensated PerkinElmer PYRIS Diamond differential scanning calorimeter (DSC) under Ar atmosphere in a graphite crucible. One DSC measurement consisted of constant heating to 873 K (600 °C) and subsequent cooling with a rate of 10 and 20 K/s in the temperature range of 873 K to 673 K (600 °C to 400 °C).

For microstructure studies, the ribbons in as-melt-spun condition and after DSC heating were carefully ground. Some ribbons were electro-polished with an electrolyte of 1/3 parts HNO_3 and 2/3 parts methanol on a LectroPol-5 at 273 K (0 °C) for scanning electron microscopy (SEM) investigations using a Zeiss Supra 55 FE-SEM. Eutectic droplet size distributions were generated by image analysis of secondary electron images taken from ribbons after DSC heating using an FEI Quanta 200 ESEM. At least 100 measurements were performed for a statistically reliable analysis. The composition of eutectic droplets in ribbons after DSC heating was further investigated with element mappings on a JEOL JXA-8500F electron probe micro analyzer (EPMA) equipped with wavelength dispersive X-ray spectrometers (WDS).

Ribbons for transmission electron microscopy (TEM) observation in the as-melt-spun condition and after DSC heating were prepared by standard metallographic procedures and dimpled to about 30 μm. A Gatan Precision Ion Polishing System (PIPS, Gatan model 691) equipped with a cold stage was used in order to maintain a constant temperature of 263 K (−10 °C) during ion beam polishing. TEM investigations were performed on an image-side Cs-corrected JEOL-2100F operated at 200 kV. The small beam diameter of the JEOL-2100F (less than 0.2 nm) makes it possible to measure the composition of trace elements (*i.e.*, Ca, P) at the Si re-entrant edges.

The ThermoCalc software with the TTAL5 database was used to calculate the solidification path and the formation temperatures of intermetallic phases in Al-5Si alloys with 25 and 250 ppm Ca additions.

III. RESULTS

A. *The As-Cast Microstructure After Conventional Casting*

Figure 1 shows representative eutectic microstructures of Al-5Si alloys with combined additions of Ca and P after conventional casting. The microstructure of the reference alloy (Figure 1(a)) is comprised short, closely spaced Si platelets and a few larger Si lamellae. A similar refined microstructure was maintained after the addition of 25 ppm Ca (Figure 1(b)). However, as the P concentration is increased to 3 and 10 ppm, the eutectic Si becomes coarse and flake-like (Figures 1(c) and (d)). In contrast, increasing the Ca concentration from 25 to 250 ppm leads to a fine plate-like eutectic Si, as shown in Figures 1((e) and (f)). Although some regions seem to undergo a slight coarsening compared to the eutectic Si in Figure 1(b), the eutectic Si in Figure 1(f) is significantly refined compared to that in Figure 1(c). Therefore, it seems that the coarsening effect of P can be significantly neutralized with the addition of 250 ppm Ca to Al-5Si alloys containing 3 ppm P. With increasing P addition from 3 to 10 ppm, coarse flake-like Si is the dominating morphology in Al-5Si alloys even with 250 ppm Ca addition. This implies that the addition of 250 ppm Ca cannot neutralize the coarsening effect imposed by higher P concentrations. It should be emphasized that an intermetallic phase with a polyhedral morphology precipitated in Al-5Si alloys with 250 ppm Ca addition independent of the P concentration. This intermetallic phase was typically located in the eutectic adjacent to primary Al dendrites. EDS analyses (not shown here) identified this phase as Al_2Si_2Ca based on their stoichiometry of 40:40:20 (at. pct).

B. *Melt-Spun Microstructure and Eutectic Droplet Size Distribution After Melt Spinning*

Figure 2 shows the typical microstructure of the Al-5Si reference alloy before and after DSC heating. Before DSC heating (Figure 2(a)), Al grains are of fine scale and equiaxed. Si crystals are present at the Al grain boundaries and in addition, a large fraction of Si crystals also resides within the Al grains. After DSC heating (Figure 2(b)), two different Si morphologies were observed. Large plate-like Si crystals were located both along the grain boundaries and inside the Al grains. Eutectic droplets with extremely fine Si particles were embedded in the Al matrix (entrained droplets). Figure 2(c) shows a representative eutectic droplet with coarser Si crystals located at the interface resembling a shell between the Al matrix and the eutectic droplet encapsulating randomly distributed fine Si crystals. For comparison, the microstructure of an Al-5Si alloy with 25 ppm Ca and 3 ppm P addition is shown in Figure 2(d). Again, Si is located at the grain boundaries and inside the Al grains. The majority of the Si in the eutectic droplets, however, coarsened to an extent that one individual eutectic droplet consisted of only a few large Si platelets.

Figure 3 shows the microstructure in Al-5Si alloys with 250 ppm Ca and different P additions after DSC heating. In particular, it documents a gradual change of the size of the eutectic droplets and the morphology of the eutectic Si. A careful analysis of droplets in the alloys containing 0.5 and 3 ppm P (Figures 3(a) and (b)) indicates an equal mixture of perfectly spherical and elliptic droplets comprised fine Si crystals.

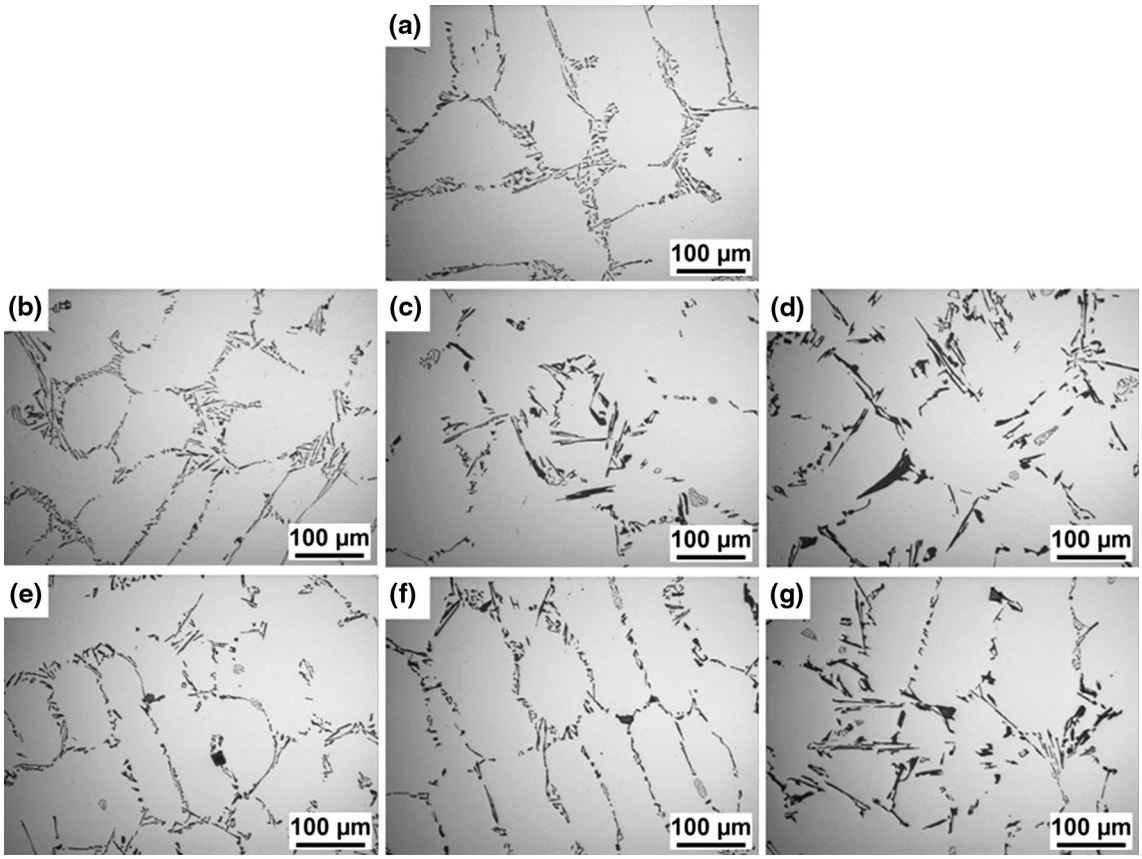

Fig. 1—Representative eutectic microstructures of QuiK-cup samples of (*a*) a Ca and P lean Al-5 Si reference alloy and of samples containing ((*b*) through (*d*)) 25 ppm Ca and ((*e*) through (*g*)) 250 ppm Ca with the P concentration increasing in a row from 0.5, 3 to 10 ppm P, respectively.

In contrast, droplets in the alloy with 10 ppm P and 250 ppm Ca (Figure 3(c)) are either small and of spherical shape, or large and of irregular shape. A dramatic coarsening of the Si inside the droplets resulting in a transition from fine Si crystals to a few large Si platelets was also observed. Figure 3(d) shows that even as the Si generally becomes coarser, the pattern of Si crystals resembling a shell at the Al matrix-droplet interface encapsulating the Si crystals in the droplets is still maintained, but these droplets obviously possess a smaller average diameter compared to droplets in P lean alloys. It is evident from the micrographs that a definite size distribution of eutectic droplets exists within the ribbons.

Figure 4 shows the droplet size distributions obtained from image analysis of a series of secondary electron images. The diameter of the eutectic droplets in the reference alloy (Figure 4(a)) ranged from 5 to 55 μm with a mean diameter of 26.9 μm, and the size distribution appears to follow the Gaussian bell curve. Similar histograms were obtained for the alloys with 0.5 ppm P and 25 ppm Ca (Figure 4(c)) and for 0.5 ppm P, 3 ppm P, and 250 ppm Ca in Figures 4((b), (d), and (e)), respectively. A shift to lower average diameters was observed when the alloys contained 3 ppm P and 25 ppm Ca, and 10 ppm P and 250 ppm Ca. While there still exists a Gaussian distribution in Figure 4(e), the histogram in Figure 4(f) exhibits an almost bimodal distribution. The latter is a direct result of the aforementioned difference in droplet geometries as described for Figure 3(c). It should be noted that it was not possible to obtain a droplet size distribution for the alloy with 25 ppm Ca and 10 ppm P. Due to the severe coarsening of the Si crystals, the former regions of fine scale eutectic droplets consisted of patches of a few large Si platelets similar to the morphology of the grain boundary eutectic and thus could not be analyzed with a sufficient accuracy. However, these results strongly indicate that increasing P concentrations lead to an increase of the fraction of smaller droplets and a significant coarsening of the Si crystals itself, as shown in Figure 3(c). The fact that an increase of the Ca concentration from 25 to 250 ppm in alloys with 3 ppm P increases the mean average diameter from 21.8 to 26.1 μm provides further evidence that Ca counteracts the coarsening effect of P, which is completely consistent with the observations during conventional casting (Figure 1).

C. *Undercooling of Eutectic Droplets After Melt Spinning*

Figure 5 shows a series of DSC traces obtained from the ribbons after DSC heating. Two distinct exothermic

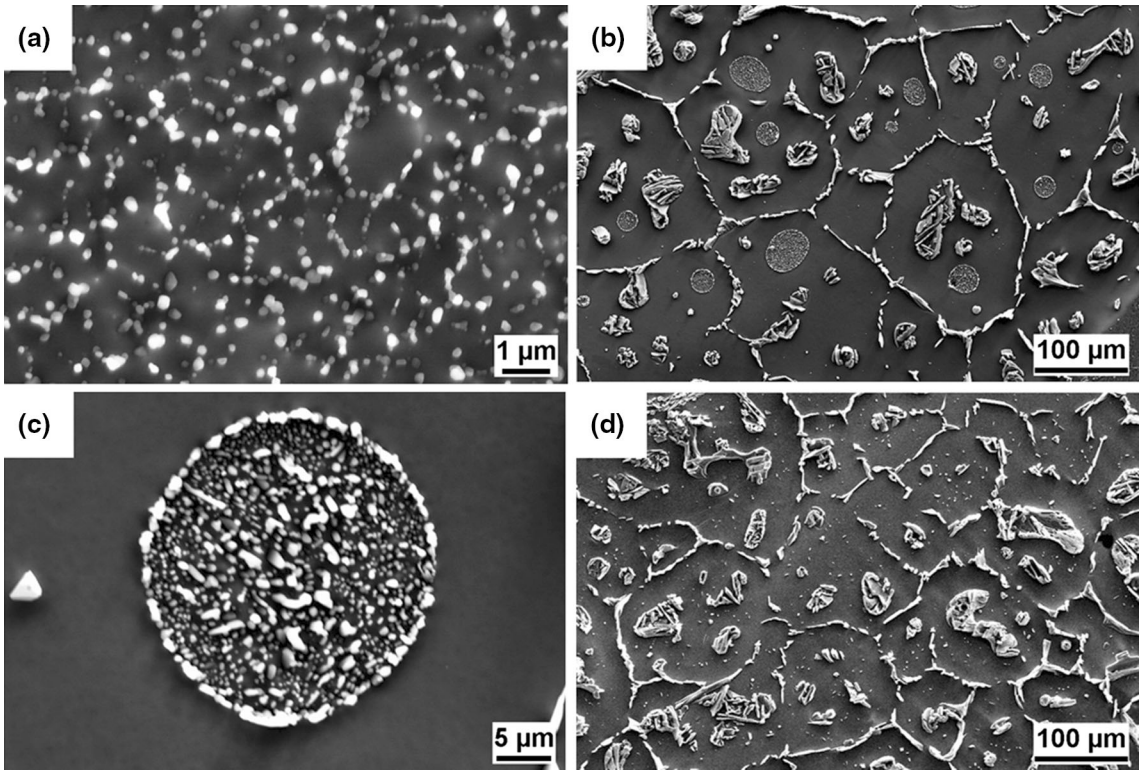

Fig. 2—Secondary electron images of the Al-5Si reference alloy. (*a*) In melt-spun condition, and (*b*) after DSC heating, showing the structure of Al grains and the distribution of the eutectic droplets. (*c*) Enlarged eutectic droplet from the same alloy. For comparison, (*d*) Al-5Si alloy with 25 ppm Ca and 3 ppm P after DSC heating, possessing a coarser droplet structure.

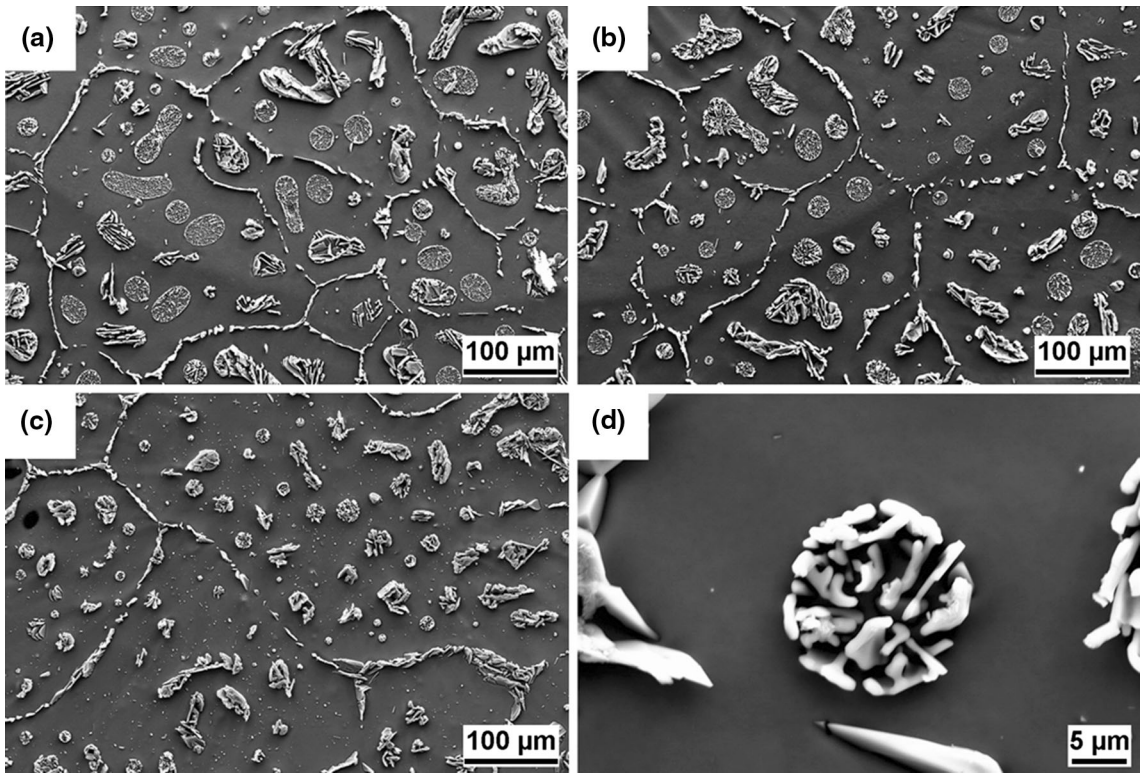

Fig. 3—Representative secondary electron images of microstructures of the Al-5 Si alloys with combined additions of 250 ppm Ca and (*a*) 0.5 ppm P, (*b*) 3 ppm, and (*c*) 10 ppm P, respectively. (*d*) Enlarged eutectic droplet from a sample with 250 ppm Ca and 10 ppm P.

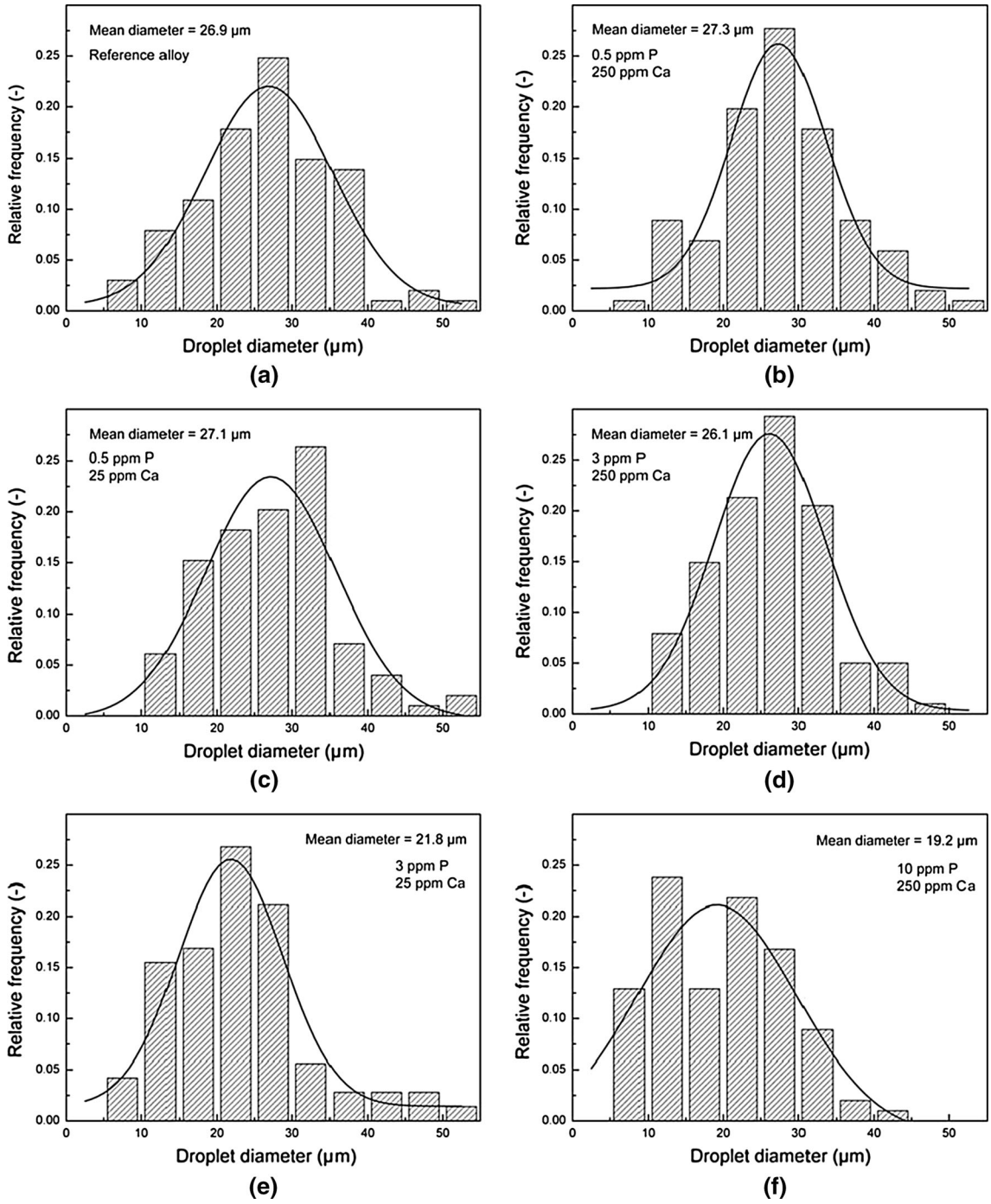

Fig. 4—The droplet size distribution in Al-5Si alloys with the combined Ca and P additions after DSC heating. Histograms are shown for (*a*) the Al-5Si reference alloy, and for alloys either with combined additions of 25 ppm Ca and (*c*) 0.5 ppm P, (*e*) 3 ppm P, or with combined additions of 250 ppm Ca and (*b*) 0.5 ppm P, (*d*) 3 ppm P, (*f*) 10 ppm P, respectively. Due to a drastic coarsening of the eutectic droplets, the size distribution for a combined addition of 25 ppm Ca and 10 ppm P could not be measured.

peaks can easily be identified. Exotherm A corresponds to the solidification of the grain boundary eutectic (Figure 2(a)). It normally occurred at an onset temperature of 847.2 K ± 0.4 K (574.2 °C ± 0.4 °C), approximately 3 K below the equilibrium eutectic solidification temperature of 850 K (577 °C). Exotherm B is associated with the solidification of eutectic droplets embedded in the Al matrix with an onset temperature typically a few degrees below the end temperature of exotherm A. The undercooling of the eutectic droplets ΔT can then be defined as the difference between the onset temperatures of exotherm A and B, as summarized in Table II. For the Al-5Si reference alloy, the undercooling is measured to be about 12.6 K (Figure 5(a); Table II). No

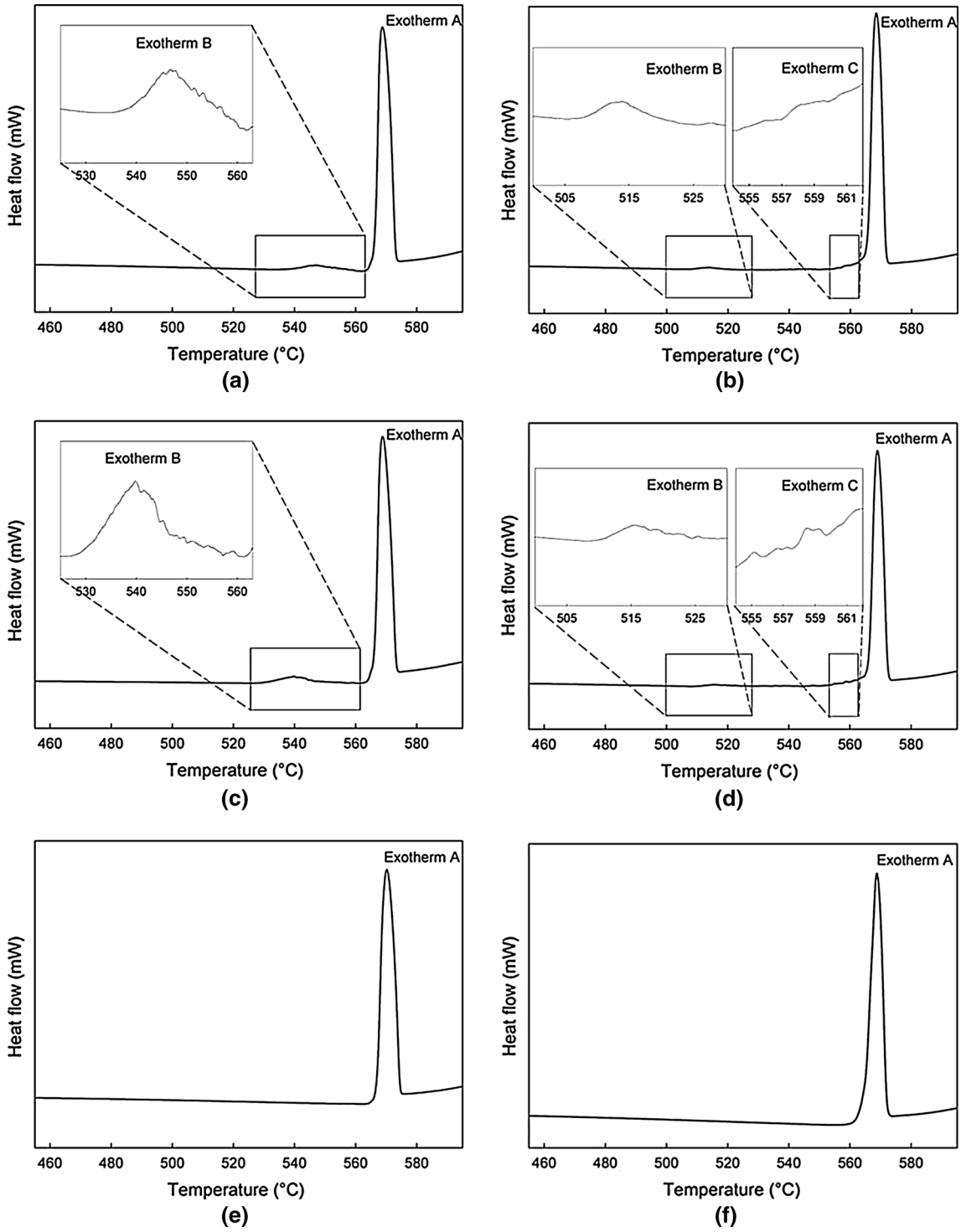

Fig. 5—DSC solidification traces after cooling with a constant rate of 10 K/s, showing the exothermic reactions for (*a*) Al-5Si reference alloy and alloys containing (*c*) 25 ppm Ca and 0.5 ppm P, (*e*) 25 ppm Ca and 3 ppm P, (*b*) 250 ppm Ca and 0.5 ppm P, (*d*) 250 ppm Ca and 3 ppm P, (*f*) 250 ppm Ca and 10 ppm P. Exothermic reactions corresponding to the solidification of eutectic droplets (Exotherm B) and to the precipitation of the Al_2Si_2Ca phase (Exotherm C) are enlarged for clarification.

significant change of the undercooling (13.1 K, Table II) was observed with the addition of 25 ppm Ca (Figure 5(c)). However, when the P concentration is increased above 0.5 ppm (*i.e.*, 3 and 10 ppm P), exotherm B disappears (Figure 5(e)). This agrees well with our previous report,[30] where 3 to 4 ppm P addition to an Al-5Si alloy leads to a displacement of the exotherm B toward exotherm A suggesting that the eutectic droplets in these alloys nucleated with negligibly small undercoolings. Even though the histogram in Figure 4(e) shows a distribution of droplets, the overall number density of eutectic droplets in the ribbons might

Table II. Undercooling of Eutectic Droplets in Melt Spun Ribbons Measured by DSC, and Undercooling of the Al-Si Eutectic Reaction Obtained from Thermal Analysis with the QuiK-Cup® Method

Ca (ppm)	P (ppm)	ΔT for Constant Cooling at 10 K/min (K)	ΔT for Constant Cooling at 20 K/min (K)	ΔT_{eu} for Conventional Casting, Cooling Rate 10 K/min (K)
0	0.5	12.6	19.2	3.2
25	0.5	13.1	19.5	3.2
	3.0	—	—	0.9
	10	—	—	0.8
250	0.5	48.6	49.9	3.6
	3.0	49.1	47.6	3.7
	10	—	—	3.2

The measurement of droplet undercoolings of alloys with high P concentrations was not possible (as marked with an underlined line), due to a shift of the onset temperature of exotherm B close to the onset temperature of exotherm A.

be too small to cause a detectable exotherm in the corresponding DSC trace (Figure 5(e)).

When the Ca concentration is increased to 250 ppm, another exotherm C appears in the DSC traces at an onset temperature of 833.2 K ± 0.5 K (560.2 °C± 0.5 °C) (Figures 5(b) and (d)). The exotherm C represents the formation of the Al_2Si_2Ca intermetallic phase immediately after the solidification of the inter-connected grain boundary eutectic. Moreover, the undercooling of the entrained eutectic droplets was significantly increased from 12.6 K (Al-5Si reference alloy) to 48.6 K and 49.1 K in Al-5Si alloys with additions of 250 ppm Ca and 0.5 ppm P, 3 ppm P, respectively (Table II). In these cases, the nucleation of eutectic droplets seems to be more difficult. For the Al-5Si alloy with the addition of 250 ppm Ca and 10 ppm P, again the exotherm B disappears (Figure 5(f)). Clearly, the nucleation of the eutectic Si was promoted by the high P concentration in the corresponding ribbons.

The same trend within the droplet undercooling was confirmed by measurements with a higher cooling rate of 20 K/s (Table II). The onset temperature of exotherm B is displaced to slightly lower temperatures and leads to undercoolings of about 19.2 K of the reference alloy. The undercooling of eutectic droplets of alloys with additions of 250 ppm Ca and 0.3, 3 ppm P remains unaffected, probably due to the dominating effect of 250 ppm Ca. In contrast to the low Ca addition (25 ppm Ca), the undercooling of eutectic droplets can be measured in the case of 250 ppm Ca addition even with the presence of 3 ppm P. However, the undercooling could not be assessed when 10 ppm P was added independent of the Ca concentration. This underlines that even trace additions of P have a substantial effect on the nucleation of eutectic Si in Al-Si alloys.

D. *Undercooling of the Al-Si Eutectic After Conventional Casting*

For comparison, also the recalescence undercooling of the eutectic reaction of conventional cast samples was measured (Table II). A smaller undercooling (*i.e.*, 3.2 K for reference Al-5Si alloy) was observed compared to the undercooling of eutectic droplets after melt spinning. Clearly, there is a large difference between these two solidification processes, and although the undercoolings cannot directly be compared, a similar trend was noticed. P additions generally decrease the undercooling significantly from 3.2 to 0.8 K in Al-5Si alloys with the addition of 25 ppm Ca. In contrast, 250 ppm Ca addition seems to neutralize the effect of P addition. The recalescence undercooling remains unchanged at ~ 3.6 K (for 0.5 and 3 ppm P) and is only marginally decreased to 3.2 K in the Al-5Si alloy with the addition of 10 ppm P.

E. *Electron Probe Micro-analysis*

EPMA was employed to measure the element concentration within eutectic droplets. Figures 6(a) and (b) show the WDS X-ray mappings for Al-5Si alloys with the additions of 25 ppm Ca, 250 ppm Ca, and 3 ppm P, respectively. In both cases, the eutectic droplet consisted of randomly distributed fine scale eutectic Al and Si. Traces of Ca embedded into the fine scale Al-Si eutectic were detected in the Al-5Si alloy with the 250 ppm Ca. However, P, which is presumably located at the interface between matrix Al and Si, was not detected in the present investigation due to the resolution constraints of the EPMA technique.

F. *Scheil Simulation of the Solidification Path*

Figure 7 shows the Scheil simulations of the solidification path of Al-5Si alloys with the additions of (a) 0 ppm, (b) 25, and (d) 250 ppm Ca. Figures 7((c) and (e)) shows the weight fraction of the Al_2Si_2Ca phase. The precipitation of Al_2Si_2Ca in alloys with 25 ppm Ca is predicted at about 855 K (582 °C) (Figure 7(c)), slightly higher than the eutectic temperature [850 K (577 °C)]. An increase of the Ca concentration to 250 ppm Ca results in the precipitation of Al_2Si_2Ca at 880 K (607 °C) (Figure 7(e)). Consequently, a larger weight fraction of Al_2Si_2Ca should form in these alloys. It is emphasized that in both cases, α-Al is still the primary phase.

G. *TEM Investigation on Ribbons Before and After DSC Heating*

Figure 8(a) shows a TEM bright field image of the Al_2Si_2Ca phase located between two separate Si

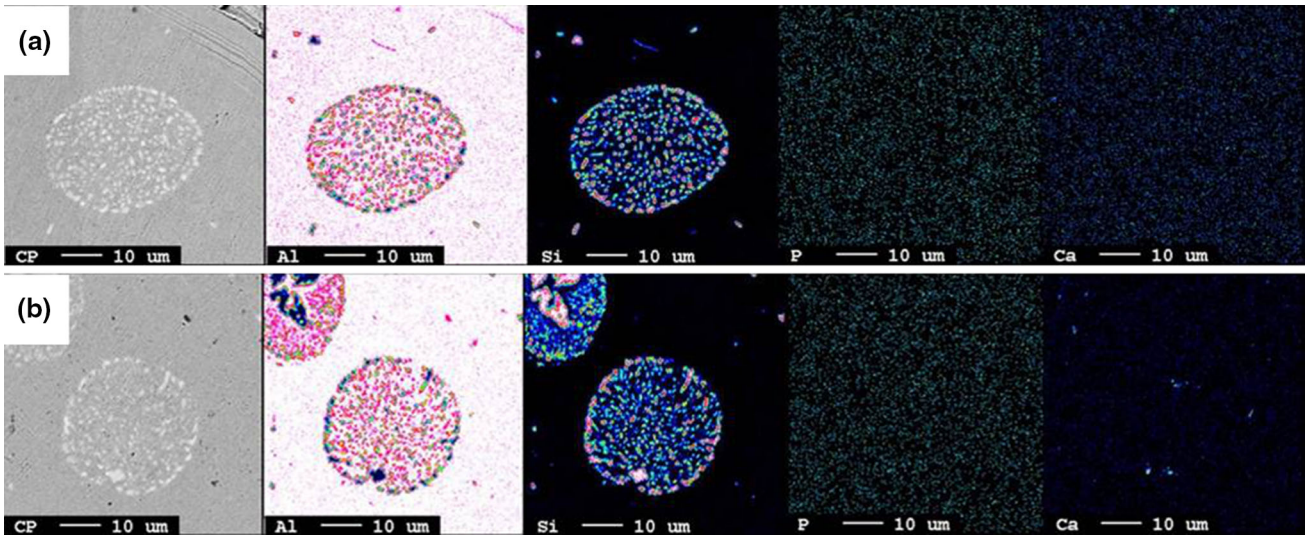

Fig. 6—EPMA element mapping of eutectic droplets after DSC heating within Al-5Si alloys with the addition of (*a*) 25 ppm Ca and 3 ppm P, and (*b*) 250 ppm Ca and 3 ppm P.

particles within the grain boundary eutectic in an alloy with the addition of 250 ppm Ca and 10 ppm P after DSC heating. The EDS analysis indicates that its stoichiometry is close to 2:2:1 (Figure 8(b)). This observation is consistent with the Scheil simulations in Figure 7, and it also indicates the presence of the Al_2Si_2Ca phase in the DSC traces of alloys containing 250 ppm Ca (Figures 5(b) and (d)). Furthermore, the EDS analysis of the Al_2Si_2Ca phase also detected traces of P. It can be argued that this P enrichment in the Al_2Si_2Ca phase has some potential to deplete the melt of P. And it is due to this possible deactivation of the few potential nucleation sites (AlP particles) in alloys with lower P concentration, in combination with a different local equilibrium in the melt-spun ribbons and the partial remelting during DSC heating, that the Al_2Si_2Ca phase precipitated after the grain boundary eutectic marking a definite exotherm C of latent heat release (Figures 5(b) and (d)).

Figure 9 shows a series of representative Si particles in melt-spun Al-5Si alloys with combined additions of Ca and P. Figures 9((b), (d), and (f)) are magnifications from Figures 9((a), (c), and (e)) to show the details at the re-entrant edge. The Si particles were tilted to the principal twinning orientation of Si ($\langle 011 \rangle$). Viewed from the $[011]_{Si}$ zone axis, each Si particle appears to be multiply twinned. This observation is in contrast to previous reports in melt-spun Al-5Si alloys without trace element additions,[31] where most Si twins were grown along one special plane (*i.e.*, $\{111\}_{Si}$), rather than multiply twinned. This indicates that the presence of Ca promotes a significant Si twinning in the presence of high cooling rates. However, it should be noted that increasing the Ca concentration from 25 ppm (Figures 9(a) and (b)) to 250 ppm (Figures 9(c) and (d)) appears to decrease the number density of twinned Si particles. In particular, it reduces multiple twinning in Si particles when the P concentration remains constant at 0.5 ppm. This is most evident when comparing Figure 9(b) with Figure 9(d). By increasing the P addition from 0.5 ppm (Figures 9(c) and (d)) to 10 ppm (Figures 9(e) and (f)) in the presence of 250 ppm Ca, no significant changes on Si twinning are observed but the Si particles become larger. The number density of Si twins appears to be decreasing compared to the case of 25 ppm Ca addition (Figures 9(a) and (b)). This decrease in number density caused by Ca addition is very different from the increase in number density caused by Sr and/or Na addition, implying that a different behavior may occur, and other parameters influencing the Si twinning (*i.e.*, partition behavior of Ca in Si) should also be considered. However, some defects (*i.e.*, solute clustering) were observed in the vicinity of the re-entrant edge, as marked with a white arrow in Figure 9(f). EDS analysis using nanobeam mode (Figure 9(g)) shows that traces of Ca and Cu are present in this area. As described in the experimental methods, the beam diameter is small enough (less than 0.2 nm) to measure the composition of trace elements (*i.e.*, Ca, P) at the re-entrant edge. The presence of the Cu peak can be attributed to Al-Cu-P master alloy, which is used for the P addition, while the presence of the weak Ca peak may be due to segregation effects of Ca during melt spinning. Here, it should be noted that the presence of Ca was only observed in the vicinity of the re-entrant edge, where some defects were also present. Ca, even at a very low concentration, could not be measured at any other defect free region or re-entrant edge of the Si platelets, such as in Figures 9(b) and (d). This signifies that Ca may predominantly diffuse away from the advancing solid–liquid Si interface during melt spinning. In summary, the observed Si twins, can be attributed to (i) higher cooling rates during melt spinning, and (ii) the partitioning of Ca into Si (if any), which promotes the formation of multiply twinned Si particles.

The same alloys were investigated after DSC heating. A side effect of DSC is that the eutectic droplets grew by ripening from about 0.05 μm (melt-spun condition, Figure 9) to 5 μm (Figure 10). A representative low

magnification image displaying a larger Si particle is shown in Figure 10(e). The Si crystals appear to have a plate-like morphology, similar to the eutectic structures in Figure 1. Si twinning was still observed, although the number density of twins is reduced compared to Si twinning in melt-spun condition. More importantly, most Si twinning was grown with a special $\{111\}_{Si}$ (Figures 10(b), (d), and (f)), rather than being multiple twinned (Figures 9(b), (d), and (f)). This is, again, in contrast to the case of Sr and Na addition, where multiple twinned Si is present even after DSC heating. Clearly, there seems to be a different behavior in the interaction between Ca and Si, and Sr, Na, and Si in Al melts.

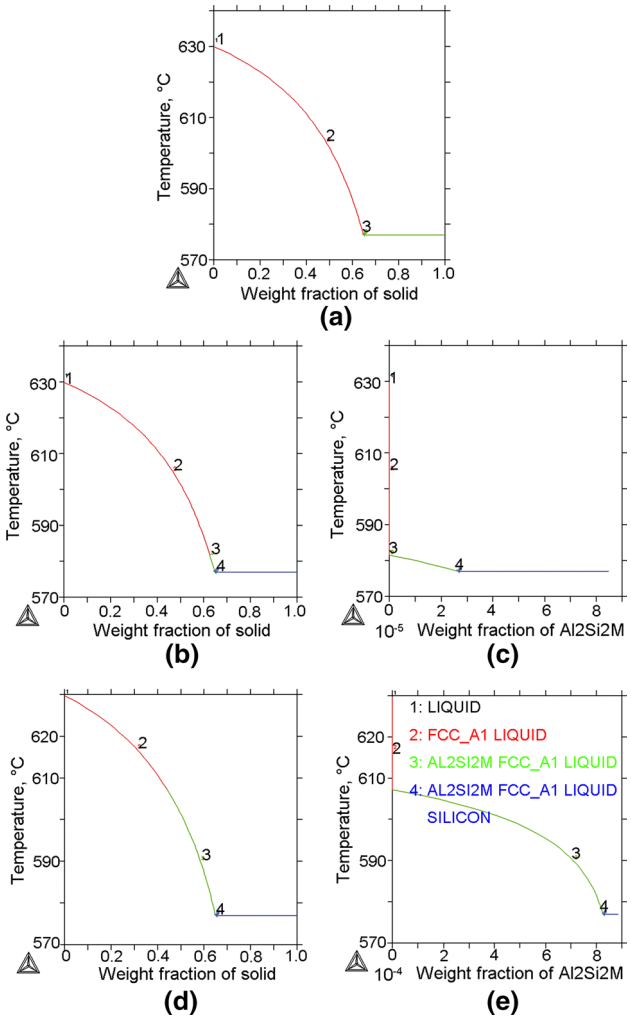

Fig. 7—Scheil simulation of the solidification sequence of Al-5Si alloys with the additions of (*a*) 0 ppm, (*b*) 25, and (*d*) 250 ppm Ca. (*c*) and (*e*) show the weight fraction of the Al_2Si_2Ca phase.

Certainly, in both cases, the number density of Si twins decreases, whereas the width of Si twins increases. It should be noted that during DSC heating, the heating and cooling rates are similar to the conditions during conventional casting, which have commonly been investigated. Thus, it can be expected that Ca additions will not yield multiple twinned Si after conventional casting. On the other hand, Sr additions to Al-Si alloys cause multiple Si twinning and result in a fibrous eutectic Si, also after conventional casting (sand casting and/or die casting). Therefore, these results imply a rather neutral effect of the Ca additions on the eutectic Si in the present study.

IV. DISCUSSION

A. *Refinement Mechanisms of Eutectic Si for Conventional Casting*

From an analysis of the optical micrographs of conventional cast samples in Figure 1, it is clear that a refined rather than a fully fibrous morphology can be achieved in a HP Al-5 wt pct Si alloy with additions of Ca to P containing alloys. The most refined structure is the one of a P and Ca lean reference alloy. This refinement is consistent with reports on Yb, Y, and Sb additions to hypoeutectic Al-Si alloys. However, it is different from the modification commonly achieved with Sr and Na addition. It seems to be of great importance to distinguish between refinement and modification of the Al-Si eutectic. It is well accepted that refinement is defined as an decrease in eutectic Si size from coarse to

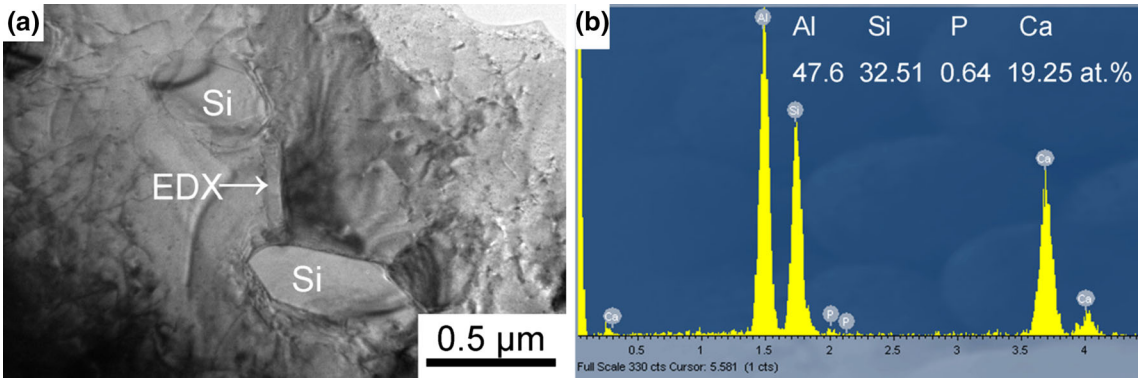

Fig. 8—TEM bright field image (*a*) and EDX analysis (*b*) taken from the area (as marked with a white arrow in (a)) in Al-5Si-based alloy with the addition of 250 ppm Ca and 10 ppm P after DSC heating, showing the presence of the Al_2Si_2Ca phase. The P peak may be related to the interaction between Ca and P.

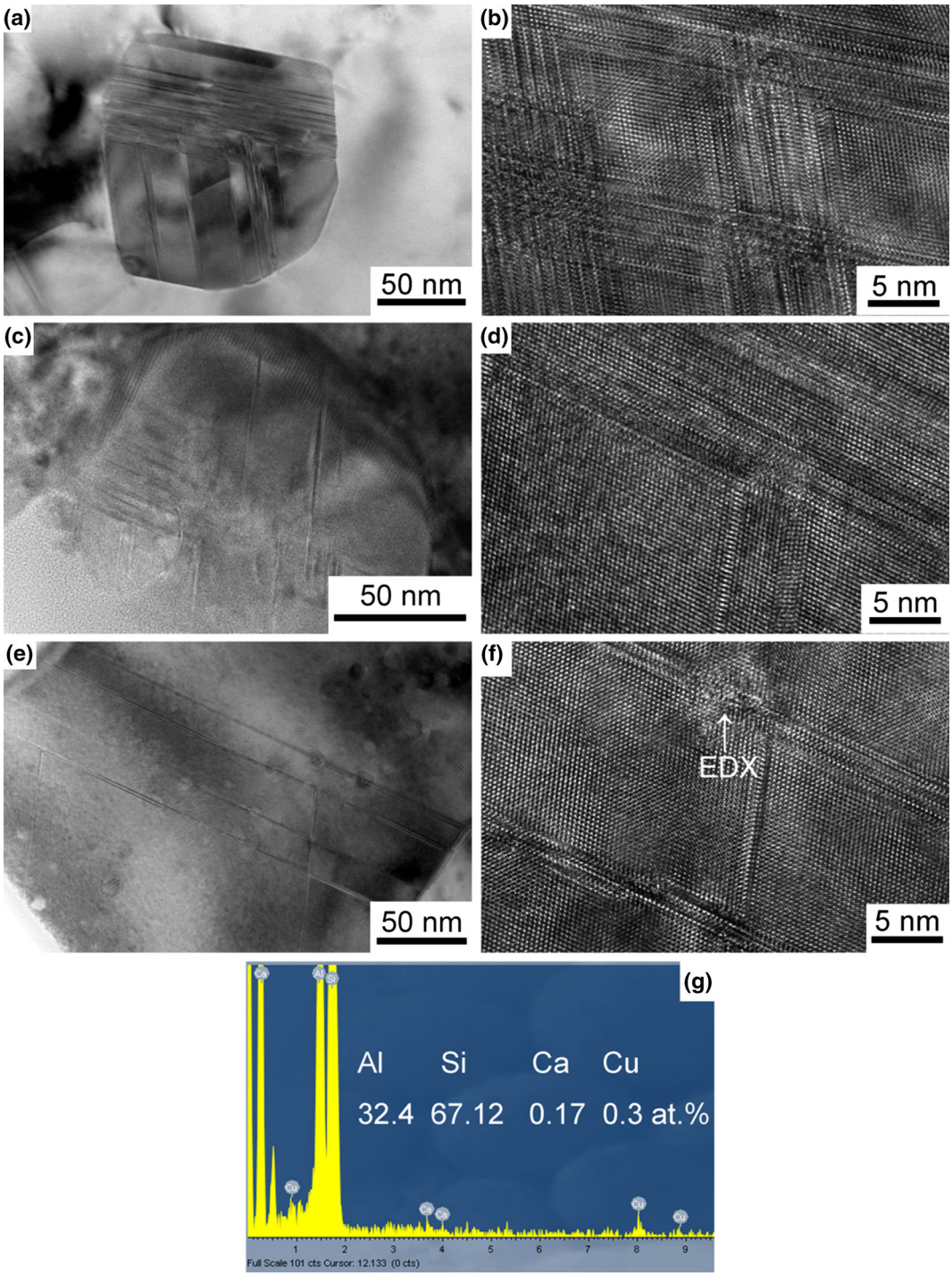

Fig. 9—TEM bright field images taken from melt-spun Al-5Si-based alloys with the additions of (*a*) and (*b*) 25 ppm Ca and 0.5 ppm P, (*c*) and (*d*) 250 ppm Ca and 0.5 ppm P, (*e*) and (*f*) 250 ppm Ca and 10 ppm P. (b), (d), and (f) are enlarged from (a), (c), and (e), respectively. EDS analysis (*g*) was taken from the area, as marked in (f). The Cu peak can be attributed to Al-Cu-P master alloy used for P addition, while the weak Ca peak may be due to the trapping of Ca during melt spinning. (B//[011] $_{Si}$).

fine platelets, while modification is defined as a change of the Si morphology from plate-like to fibrous. In addition, refinement is normally related to changes of Si nucleation, whereas modification is associated with alterations during the growth of eutectic Si, even though they cannot be regarded independent of each other.

For nucleation of eutectic Si, the P concentration is one of the most important parameters that must be carefully monitored. At a low P concentration, *e.g.*, in HP Al-5Si alloys, fine plate-like eutectic Si can be observed (Figure 1(a)). Increasing the P additions to 10 ppm even with the presence of 25 ppm Ca caused a

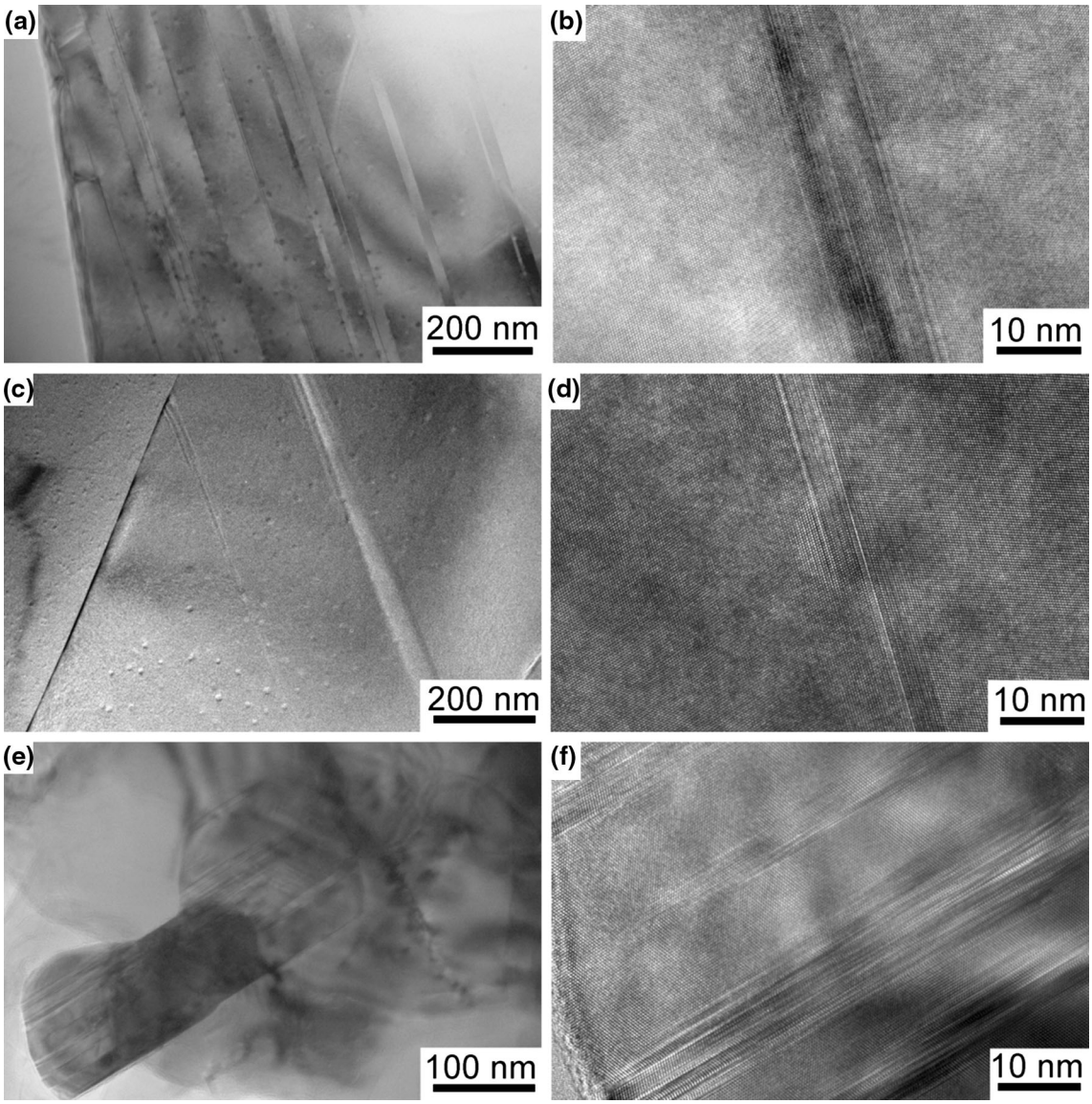

Fig. 10—TEM bright field images taken from the Al-5Si-based alloys after DSC heating with the additions of (*a*) and (*b*) 25 ppm Ca and 0.5 ppm P, (*c*) and (*d*) 250 ppm Ca and 0.5 ppm P, (*e*) and (*f*) 250 ppm Ca and 10 ppm P. (b), (d), and (f) are enlarged from (a), (c), and (e), respectively. Si twinning was still observed, although most Si twinning was grown with a special $\{111\}_{Si}$, rather than multiply twinned. (B//[011] $_{Si}$).

change from fine plate-like to a coarse flake-like eutectic Si structure. With 250 ppm Ca added to alloys containing up to 3 ppm P, this coarsening could efficiently be counteracted. Again, a coarse flake-like eutectic Si structure is obtained in alloys with 10 ppm P and 250 ppm Ca. The main reason for the counteraction by Ca additions may be an alteration of the macroscopic growth of eutectic grains.

A detailed description of the macroscopic growth modes can be found elsewhere.[32,33] In our previous work,[34] the threshold levels for the transition of the macroscopic growth mode with respect to P were identified in a HP Al-7Si alloy. It was shown that a change of the macroscopic growth mode from nucleation at the mold wall followed by growth with a strong dependence on the thermal gradient to nucleation on impurity particles, most likely AlP, in the vicinity of the primary Al dendrites takes place when between 2 and 3 ppm P are added. This results in a dramatic increase in the nucleation frequency of eutectic grains. As an increase of the nucleation frequency can directly be related to an increase of the average surface area of eutectic grains, the eutectic solid–liquid interface advances slower for a given constant rate of heat transport out of the system.[23] AlP particles are suggested to promote the nucleation of eutectic Si, and the amount of undercooling is reduced[22,34,35] whereas the time for solute diffusion is increased resulting in a coarsening of the eutectic Si crystals. On the other hand, this effect can be neutralized when sufficient Ca is added (Figure 1). In a recent publication,[36] it is shown that Ca additions to HP Al-7Si alloys with P concentrations typically found

in commercial hypoeutectic Al-Si alloys in the range of 5 to 20 ppm; the macroscopic growth mode of the eutectic grains is reversed again. The eutectic then evolves from the mold walls toward the center of the casting with a distinct growth front. This change in growth mode is further substantiated by Ca additions to a commercial purity A356 alloy reported by Nogita *et al.*[37] The resultant refinement of the eutectic Si in the conventional cast samples might then be attributed to the higher undercooling that needs to be provided due to the possible deactivation of P-rich nucleants in the melt, presumably AlP, by the Ca addition.

B. *Refinement of the Eutectic Droplet Size After Melt Spinning*

Not only for conventional casting, also during melt spinning, P and Ca additions were observed to have significant influence on the nucleation temperature and the microstructure of the ribbons, *i.e.*, size and distribution of the eutectic droplets. With high droplet undercooling of 13 K and 49 K as in alloys with up to 3 ppm P, and 25, 250 ppm Ca, respectively, the droplets solidified with a large number of non-faceted Si crystals and few coarser Si crystals were found to be located at the matrix-droplet interface (0.5 ppm P in Figure 2(c)),. At a high P concentration (10 ppm P in Figure 3(d)), even with the presence of 250 ppm Ca, the droplets solidified with a significantly lower number of non-faceted Si crystals and fewer coarse Si crystals were found to be located at the matrix-droplet interface. In addition, a large fraction of the droplets in these alloys were comprised one or a few large Si platelets. It is generally accepted that Si does not nucleate on the Al matrix which surrounds the droplets[38] in the presence of trace amounts of impurities adsorbed on the Al interface as AlP. At P concentrations higher than 2 ppm, Ho and Cantor[35,39] report P containing particles (AlP) at the Al matrix-droplet interface as the source for the nucleation of the coarser Si crystals on the periphery of the droplets at significantly lower undercoolings. At low P concentration lower than 2 ppm, Ho and Cantor[35,39] predicted AlP adsorbed at the Al matrix-droplet interface. This is followed by rapid multiple nucleation events resulting in fine non-faceted Si crystals, as shown in Figures 2 and 6.

The exotherm corresponding to the solidification of eutectic droplets disappeared when the P concentration in the present investigation was raised to 10 ppm irrespective of the Ca concentration. Most likely it overlapped with the exotherm of the grain boundary eutectic indicating that little or no undercooling is needed for the droplet nucleation. In this case, the majority of droplets in the class size 15 to 45 μm were comprised coarse-faceted Si crystals and few droplets with fine scale non-faceted eutectic Si constituted the class size 10 to 15 μm (Figures 3(d)). A closer inspection of the size distribution revealed a transition from a Gaussian to an almost bimodal distribution due to these geometrical effects. Representative microstructures in Figures 3((a) through (c)) suggest that P generally decreases the average droplet diameter and lead to a significant coarsening of the Si in the majority of the droplets. The shift of the droplet exotherm with decreasing alloy purity, *i.e.*, predominantly with increasing P concentration, is in excellent agreement with the nucleation theory in liquid droplets by Kim *et al.*[40] as an increase of the number of potential nucleation sites displaces the onset of the droplet exotherm to higher temperatures. Also, the change of the morphology of the Si within the droplets and the altered droplet distribution is consistent with heterogeneous nucleation theory of Si in hypoeutectic Al-Si alloys reported by Ho and Cantor.[35] It is claimed that some of the eutectic droplets contain no AlP and only P which dissolved in the course of the heating phase during DSC. When the overall P concentration in the alloy is high (larger than 0.5 ppm), also the fraction of undissolved AlP patches in the droplets is larger. In this case, Si nucleates on the pre-existing AlP patches with little undercooling simultaneously with the grain boundary eutectic and grows to coarse-faceted Si crystals. The dissolved P in the remaining droplets will then precipitate by attachment to the Al matrix at the droplet-matrix interface to form AlP which will assist Si nucleation (Figure 3(d)). It should be noted that the fraction of droplets nucleating, after the grain boundary eutectic consisting of non-faceted Si crystals, will be too small to be detected in the DSC traces. When the concentration of available P is low (*e.g.*, 0.5 to 3 ppm P or in the presence of 250 ppm Ca), most of the P will be dissolved in the melt by partial remelting during the DSC analysis, and nucleation of eutectic Si is not accelerated until Al and P recombine at the matrix-droplet interface to form AlP. This displaces the onset temperature of the eutectic droplet exotherm to significantly lower temperatures and increases the droplet undercooling. The droplets will then predominantly consist of fine scale Si (Figure 2(c)), and the droplet size distributions have a symmetrical Gaussian shape.

Although the EPMA element mappings (Figure 6) do not show the presence of P at the matrix-droplet interface, due to the low lateral resolution of the characterization technique itself, Ca was detected in the fine scale eutectic within a droplet. As discussed above, Ca additions neutralized the coarsening effect caused by P. It can be expected that the presence of Ca within the eutectic droplet also neutralizes the coarsening effect caused by P during DSC heating. Indeed, the eutectic Si within the eutectic droplet is still very fine (Figure 6(b)), compared to the Si crystals within a eutectic droplet in Figure 2(d), even with the presence of 3 ppm P.

C. *Formation of Al_2Si_2Ca and Ca_3P_2*

As predicted by the Scheil simulation, the addition of 25 ppm Ca results in the formation of the Al_2Si_2Ca phase with a low weight fraction (2.8×10^{-5}) starting close to the eutectic temperature and proceeding in a narrow solidification range of 5 K until solidification terminates in a ternary eutectic at 850 K (577 °C). No significant increase of the eutectic droplet undercooling was observed in P lean alloys (0.5 ppm P). Also, the Al_2Si_2Ca phase was not detected in conventional

castings and after melt spinning. This may be due to (i) a low number density of the Al_2Si_2Ca phase, or (ii) the Scheil simulation gives a misleading prediction because of the very different diffusion and equilibrium conditions in the two different casting processes. An increase of the Ca concentration from 25 to 250 ppm results in the formation of a larger weight fraction of the Al_2Si_2Ca phase (8.1×10^{-4}). It is predicted that precipitation starts at a higher temperature and continues over a wider solidification range. In the presence of 0.5 and 3 ppm P, a considerable increase of the droplet undercooling was observed, indicating that there is a strong interaction between Ca and P at a higher Ca concentration (250 ppm) forcing the eutectic Si to nucleate more inefficiently at larger undercoolings.

The aforementioned thermodynamic calculations show that most of the Ca is consumed by the formation of the Al_2Si_2Ca phase. It appears that the Al_2Si_2Ca phase has a similar role on the AlP particles as other ternary intermetallics of the Al_ySi_zX type, *e.g.*, Al_2Si_2Sr, Al_2SiY, and Al_2Si_2Yb detected in the alloys with Sr, Y, or Yb additions,[13,14,25,30,41] which is poisoning of the AlP phase or a reduction of P in the residual liquid of near-eutectic composition during the final stages of solidification. In a recent publication, Cho *et al.*[25] claims that the Al_2Si_2Sr phase nucleates on AlP particles. Direct experimental evidence of the interaction of Al_2SiY[14] and Al_2Si_2Yb[13] with AlP is lacking at present, but due to the pre-eutectic nature of each of the ternary phases, it is assumed that these intermetallics possess some potential for the deactivation of the AlP phase. Entrained droplet studies and the analysis of DSC traces have shown that the Al_2Si_2Sr phase precipitates before the eutectic droplets during constant cooling exhibiting a distinct exotherm.[30,41] In a similar manner, the DSC traces in the present investigation indicated the evolution of an additional exotherm C when 250 ppm Ca was added. This was accompanied with a drastic increase of the undercooling of eutectic droplets from 13 K to 49 K. TEM studies of these alloys revealed the presence of Al_2Si_2Ca intermetallics. From the EDS spectrum taken from the sample after DSC heating presented in Figure 8(b), it is evident that P was tied up in the Al_2Si_2Ca phase. In addition, quenched microstructures presented by Cho and Dahle[6] and in our previous work,[36] clearly reveal the precipitation of Al_2Si_2Ca particles ahead of the eutectic solid–liquid interface. These particles possessed centrally located distinct P-rich secondary phase particles or substantial P enrichment. It is likely that this leads to a depletion of pre-existing AlP particles or residual P in the melt. As a consequence, less active AlP particles or P for the formation of AlP was present in the solute boundary layer ahead of the solid–liquid eutectic interface and in the eutectic droplets. AlP or patches are generally accepted as the potential nucleation site for Si in hypo- and hypereutectic Al-Si alloys due their similarity in crystallography. The lattice mismatch between AlP and Si is below 1 pct[22] (AlP: zinc blende cubic, a = 5.421 Å[42] and Si: diamond cubic, a = 5.431 Å[43]).

It is argued that the formation of a binary phosphide different to AlP and Ca_3P_2 may also reduce the amount of AlP. Despite the lack of direct experimental support of the existence of Ca_3P_2 in the present investigation, the higher thermodynamic stability of Ca_3P_2 compared to AlP as discussed in Reference 44 might offer an alternative explanation for the deactivation of the AlP phase. By employing an equation presented by Turnbull and Vonnegut,[45] the disregistry of Si and Ca_3P_2 was calculated as 5.9 pct (Ca_3P_2, tetragonal, a = 5.44 Å, c = 6.59 Å.[46]), implying that Ca_3P_2 is a poor nucleant for eutectic Si compared to AlP. The Al_2Si_2Ca phase has a lattice mismatch of 8 pct with Si,[47] indicating that also Al_2Si_2Ca is not a good nucleation substrate for eutectic Si. It is therefore expected that the formation of the Al_2Si_2Ca phase and Ca_3P_2 results in the deactivation of the AlP phase when the alloy contains higher concentration of Ca (*i.e.*, 250 ppm). Thus, a significant increase of both the undercooling of eutectic droplets and the recalescence undercooling during conventional casting was measured, as summarized in Table II. However, it must be noted that this can only explain a refinement of the eutectic Si from a coarse flake-like to fine plate-like morphology due to a steeper temperature gradient ahead of the eutectic solid–liquid interface but is insufficient to yield a modification effect[48] which has been repeatedly claimed in association with Ca additions to hypoeutectic Al-Si alloys.

V. CONCLUSIONS

The influence of combined Ca and P additions on the undercooling of eutectic droplets and eutectic Si in a HP Al-5 wt pct Si alloy was investigated by the entrained droplet technique and conventional casting. P additions facilitate the nucleation of eutectic Si at lower undercoolings on impurity particles, most likely AlP. This results in a significant coarsening of the resultant eutectic microstructures and changes the droplet size distributions from a Gaussian to a bimodal shape. This effect can be counteracted with the addition of sufficient Ca to precipitate the Al_2Si_2Ca phase and preferential formation of Ca_3P_2. The Al_2Si_2Ca phase and/or the Ca_3P_2 phase consume dissolved P or deactivate AlP forcing the eutectic Si to nucleate at significantly higher undercoolings. In this case, refined plate-like Si crystals are obtained. Significant Si twinning occurred; however, this is attributed to the exceptionally high cooling rates during melt spinning. At lower cooling rates, *e.g.*, 10 K/s multiple Si twinning disappeared, and twins grew with a special $\{111\}_{Si}$ yielding plate-like Si crystals. It is inferred that Ca may diffuse away from the liquid–solid Si interface during Si growth. Thus, the hypothesis stating that atoms with an atomic radius ratio close to the ideal one lead to adsorption at re-entrant corners according to the TPRE, and IIT mechanism might not apply for the element Ca under entrained casting conditions. Therefore, we believe that the effect of Ca is mainly related to the reduction of P-rich impurities in the melt. This reduction imposes a larger undercooling for the nucleation of eutectic Si, limits its growth, and thus refines the plate-like eutectic Si structure, rather than modifies the eutectic Si to a fibrous morphology.

ACKNOWLEDGMENTS

The authors would like to thank Hydro Aluminium AS, Norway for financial support. Thomas Jaeger from Vigeland Metal AS, Norway is gratefully acknowledged for the generous supply of Al5N grade aluminum. In addition, the authors acknowledge Reinhard Pippan for granting access to the TEM facilities in The Erich Schmidt Institute of Materials Science of the Austrian Academy of Sciences.

REFERENCES

1. J.E. Gruzleski and B.M. Closset: *The Treatment of Liquid Aluminum-Silicon Alloys*, American Foundrymeńs Society, 1990.
2. S.Z. Lu and A. Hellawell: *Metall. Trans. A*, 1987, vol. 18A, pp. 1721–33.
3. S.Z. Lu and A. Hellawell: *J. Cryst. Growth*, 1985, vol. 73, pp. 316–28.
4. K. Nogita, H. Yasuda, M. Yoshiya, S.D. McDonald, K. Uesugi, A. Takeuchi, and Y. Suzuki: *J. Alloys Compd.*, 2010, vol. 489, pp. 415–20.
5. A. Knuutinen, K. Nogita, S. McDonald, and A. Dahle: *J. Light Met.*, 2001, vol. 1, pp. 229–40.
6. Y.H. Cho and A.K. Dahle: *Materials and AustCeram 2009 Conference*, Gold Coast, Australia, 2009.
7. S.S.S. Kumari, R.M. Pillai, and B.C. Pai: *J. Alloys Compd.*, 2008, vol. 460, pp. 472–77.
8. S. Kumari, R. Pillai, B. Pai, K. Nogita, and A. Dahle: *Metall. Mater. Trans. A*, 2006, vol. 37A, pp. 2581–87.
9. S.S.S. Kumari, R.M. Pillai, and B.C. Pai: *Int. Mater. Rev.*, 2005, vol. 50, pp. 216–38.
10. C.R. Loper and J.I. Cho: *AFS Trans.*, 2000, vol. 108, pp. 585–92.
11. L.F. Mondolfo: *Aluminum Alloys: Structure and Properties, IX*, Butterworths, London, 1976, p. 971.
12. A. Abdollahi and J. Gruzleski: *Int. J. Cast Met. Res.*, 1998, vol. 11, pp. 145–56.
13. J.H. Li, S. Suetsugu, Y. Tsunekawa, and P. Schumacher: *Metall. Mater. Trans. A*, 2013, vol. 44A, pp. 669–81.
14. J.H. Li and P. Schumacher: *Int. J. Cast Met. Res.*, 2012, vol. 25, pp. 347–57.
15. S. Khan and R. Elliott: *J. Mater. Sci.*, 1994, vol. 29, pp. 736–41.
16. C.J. Simensen, Ø. Nielsen, F. Hillion, and J. Voje: *Metall. Mater. Trans. A*, 2007, vol. 38A, pp. 1448–51.
17. V.D. Belov, A.V. Kurdyumov, and S.V. Inkin: *Sov. J. Non-Ferr. Met.*, 1981, vol. 9, p. 497.
18. M.B. Gokhshtein and L.S. Vasil'eva: *Met. Sci. Heat Treat.*, 1970, vol. 12, pp. 591–93.
19. H. Lescuyer, M. Allibert, and G. Laslaz: *J. Alloys Compd.*, 1998, vol. 279, pp. 237–44.
20. S.Z. Beer: *J. Electrochem. Soc.*, 1969, vol. 116, pp. 263–65.
21. S.-M. Liang and R. Schmid-Fetzer: *CALPHAD*, 2013, vol. 42, pp. 76–85.
22. K. Nogita, S.D. McDonald, K. Tsujimoto, K. Yasuda, and A.K. Dahle: *J. Electron Microsc.*, 2004, vol. 53, pp. 361–69.
23. S.C. Flood and J.D. Hunt: *Met. Sci.*, 1981, vol. 15, pp. 287–94.
24. P.B. Crosley and L.F. Mondolfo: *AFS Trans.*, 1966, vol. 74, pp. 53–64.
25. Y.H. Cho, H.C. Lee, K.H. Oh, and A.K. Dahle: *Metall. Mater. Trans. A*, 2008, vol. 39A, pp. 2435–48.
26. W. Jie, Z. Chen, W. Reif, and K. Müller: *Metall. Mater. Trans. A*, 2003, vol. 34A, pp. 799–806.
27. M. Calvo-Dahlborg, P.S. Popel, M.J. Kramer, M. Besser, J.R. Morris, and U. Dahlborg: *J. Alloys Compd.*, 2013, vol. 550, pp. 9–22.
28. C.C. Wang and C.S. Smith: *TMS-AIME*, 1950, vol. 188, pp. 136–38.
29. K.I. Moore, D.L. Zhang, and B. Cantor: *Acta Metall. Mater.*, 1990, vol. 38, pp. 1327–42.
30. M. Zarif, B. McKay, J. Li, and P. Schumacher: *BHM*, 2010, vol. 155, pp. 506–11.
31. J.H. Li, M.Z. Zarif, G. Dehm, and P. Schumacher: *Philos. Mag.*, 2012, vol. 92, pp. 3789–3805.
32. A. Dahle, K. Nogita, S. McDonald, J. Zindel, and L. Hogan: *Metall. Mater. Trans. A*, 2001, vol. 32A, pp. 949–60.
33. A.K. Dahle, K. Nogita, S.D. McDonald, C. Dinnis, and L. Lu: *Mater. Sci. Eng. A*, 2005, vols. 413–414, pp. 243–48.
34. T.H. Ludwig, P.L. Schaffer, and L. Arnberg: *Metall. Mater. Trans. A*, 2013, vol. 44A, pp. 5796–5805.
35. C.R. Ho and B. Cantor: *Acta Metall. Mater.*, 1995, vol. 43, pp. 3231–46.
36. T.H. Ludwig, E. Schonhovd Dæhlen, P.L. Schaffer, and L. Arnberg: *J. Alloys Compd.*, 2014, vol. 586, pp. 180–90.
37. K. Nogita, A. Knuutinen, S. McDonald, and A. Dahle: *J. Light Met.*, 2001, vol. 1, pp. 219–28.
38. D. Zhang and B. Cantor: *Metall. Trans. A*, 1993, vol. 24A, pp. 1195–1204.
39. C.R. Ho and B. Cantor: *J. Mater. Sci.*, 1995, vol. 30, pp. 1912–20.
40. W.T. Kim, D.L. Zhang, and B. Cantor: *Metall. Trans. A*, 1991, vol. 22A, pp. 2487–2501.
41. M. Zarif, B. McKay, and P. Schumacher: *Metall. Mater. Trans. A*, 2011, vol. 42A, pp. 1684–91.
42. C.Y. Yeh, Z.W. Lu, S. Froyen, and A. Zunger: *Phys. Rev. B*, 1992, vol. 46, pp. 10086–97.
43. M.E. Straumanis and E.Z. Aka: *J. Appl. Phys.*, 1952, vol. 23, pp. 330–34.
44. M.E. Schlesinger: *Chem. Rev.*, 2002, vol. 102, pp. 4267–4302.
45. D. Turnbull and B. Vonnegut: *Ind. Eng. Chem.*, 1952, vol. 44, pp. 1292–98.
46. B. Aronsson, T. Lundström, and S. Rundqvist: *Borides, Silicides, and Phosphides: A Critical Review of Their Preparation, Properties and Crystal Chemistry*, Wiley, Methuen, New York, NY, 1965.
47. K. Al-Helal, Y. Wang, I. Stone, and Z. Fan: *Mater. Sci. Forum*, 2013, vol. 765, pp. 117–22.
48. S.D. McDonald, A.K. Dahle, J.A. Taylor, and D.H. StJohn: *Metall. Mater. Trans. A*, 2004, vol. 35, pp. 1829–37.